Lithos 200–201 (2014) 35–48

Contents lists available at ScienceDirect

Lithos

journal homepage: www.elsevier.com/locate/lithos

Neoproterozoic chromite-bearing high-Mg diorites in the western part of the Jiangnan orogen, southern China: Geochemistry, petrogenesis and tectonic implications

Xin Chen [a], Di Wang [a], Xiao-Lei Wang [a,*], Jian-Feng Gao [b], Xu-Jie Shu [a], Jin-Cheng Zhou [a], Liang Qi [c]

[a] State Key Laboratory for Mineral Deposits Research, Department of Earth Sciences, Nanjing University, Nanjing 210093, PR China
[b] Geological Survey of Canada, 601 rue Booth Street, Ottawa, Ontario, KIA 0E8, Canada
[c] State Key Lab of Ore Deposit Geochemistry, Institute of Geochemistry, Chinese Academy of Sciences, Guiyang 550002, PR China

ARTICLE INFO

Article history:
Received 17 August 2013
Accepted 17 April 2014
Available online 30 April 2014

Keywords:
High-Mg diorite
Chromite
Geochemistry
Petrogenesis
Neoproterozoic
Jiangnan orogen

ABSTRACT

High-Mg diorites were discovered in the southern part of the ca. 830 Ma Dongma Pluton, northern Guangxi Province of southern China. The diorites (SiO_2 = 59–65 wt%) are characterized by high MgO (6.7–8.9 wt%) contents and Mg-number [Mg# = 100 × Mg/(Mg + Fe)] (69–73), in contrary to the associated medium-Mg (MgO = 3.4–3.8 wt%, Mg# = 59–63) granodiorites in the Dongma main body and the low-Mg (MgO = 1.4–1.9 wt%, Mg# = 46–51) granodiorites in the Bendong Pluton to the north. Moreover, the high-Mg diorites show surprisingly high Cr (595–640 ppm) and Ni (171–194 ppm) concentrations, which are beyond the ranges of most coeval mafic rocks in the study area. Correspondingly, chromite crystals were separated from the high-Mg diorites and some of the medium-Mg granodiorites, and they show high Cr# [100 × Cr/(Cr + Al)] (average of 75), but low Mg# (0.34–2.51) and low Fe^{3+}. The decoupling of Cr# and Mg# and the existence of quartz + apatite mineral inclusion in chromites suggest Mg-Fe exchange that may be facilitated by the disequilibrium resulted from magma mixing. The high-Mg diorites show low La/Yb (6.8–8.5) and Sr/Y (2.1–3.1) ratios, significant negative anomalies of Nb and Ti and positive anomaly of Pb, resembling the Setouchi high-Mg andesites, despite of their relatively low Sr (71–100 ppm). All of the studied diorites and granodiorites show enriched Nd isotope compositions, with $\varepsilon_{Nd}(t)$ values (−3.2 to −5.9) a bit higher than some of the associated mafic rocks. Some of the high-Mg diorites show whole-rock $\varepsilon_{Hf}(t)$ (−6.0 to −6.2) coupled with Nd isotopes, similar to the associated mafic-ultramafic rocks in northern Guangxi, suggesting the metasomatism by melts of subducting sediments in the mantle source. Whereas, others show decoupled Nd-Hf isotopes that are similar to the medium- and low-Mg granodiorites [$\varepsilon_{Hf}(t)$ = −1.8 to +0.05], probably indicating the late magma mixing with granitic magmas at a crustal level for the dioritic magmas. We propose a two-stage model for the petrogenesis of the high-Mg diorites: 1) the mantle source was firstly metasomatized by melts from partial melting of subducting terrigenous sediments to form the enriched Nd-Hf isotopic characteristics; and then 2) the mantle-derived high-Mg mafic melts mixed with the crust-derived low-Mg granitic melts to form the high-Mg diorites and medium-Mg granodiorites. The occurrence of high-Mg diorites implies the existence of Neoproterozoic subduction-related metasomatism in the western part of the Jiangnan orogen.

1. Introduction

High-Mg intermediate magmas (including andesites and diorites) are crucial to understanding the growth of continental curst that shows andesitic bulk composition (Rudnick and Fountain, 1995; Taylor and McLennan, 1981). Over the past few decades, a considerable number of studies have been made on the petrogenesis of high-Mg andesites (HMAs) (*e.g.*, Tatsumi, 2006 and references therein; Qian and Hermann, 2010; Wood and Turner, 2009). The elevated MgO contents and Mg-number (Mg#) compared to normal andesites suggest that HMA magmas may be primitive and represent near-primary magmas produced in equilibrium with the Earth's mantle (Tatsumi et al., 2006), whereas most andesites are derived from parental basaltic magmas via complex and variable processes such as crystallization differentiation, crustal contamination, anatexis of pre-existing basaltic crust and magma mixing (*e.g.*, Couch et al., 2001; Gill, 1981; Grove et al., 2003; Hildreth, 1981; Hunter, 1998; Sakuyama, 1981; Tatsumi et al., 2002; Temel et al., 1998).

The occurrence of HMAs has been reported, for example, in the Bonin Islands, Baja California, Piip volcano in W Aleutians, and the Setouchi volcanic belt in SW Japan (*e.g.*, Kuroda et al., 1978; Saunders

* Corresponding author at: State Key Laboratory for Mineral Deposits Research, School of Earth Science and Engineering, Nanjing University, Nanjing 210093, China. Tel.: +86 2589680896; fax: +86 2583686016.
E-mail address: wxl@nju.edu.cn (X.-L. Wang).

http://dx.doi.org/10.1016/j.lithos.2014.04.007
0024-4937/

et al., 1987; Tatsumi and Ishizaka, 1981; Yogodzinski et al., 1994), and they were generally named into four types, respectively, based on their unusual chemical and petrographic signatures in different areas: boninites (Kuroda et al., 1978), bajaites (Rogers et al., 1985), adakites (Defant and Drummond, 1990; Kay, 1978), and sanukitoids (Koto, 1916; Tatsumi and Ishizaka, 1981). The four types of HMAs are all related with subduction environments, requiring a melting of residual mantle or subducting oceanic crust, (Crawford et al., 1989; Defant and Drummond, 1990; Macpherson and Hall, 2001; Saunders et al., 1987; Shimoda, 2009; Shimoda et al., 1998; Stern and Kilian, 1996; Taylor et al., 1994; Yogodzinski et al., 1994, 1995) at convergent plate margins, implying a hot slab subduction (*e.g.*, Tatsumi and Maruyama, 1989). The high geothermal gradients necessary for producing HMA magmas would have been satisfied more commonly in the Archean than at present. Indeed, Archean high-Mg diorite and volcanic equivalents, and Archean analog of Cenozoic HMAs, are present in the Superior Province and Pilbara Craton and were named 'Archean sanukitoid' (Shirey and Hanson, 1984; Stern et al., 1989). However, Archean high-Mg diorites are volumetrically minor, and 60%–70% (Condie, 1981) of exposed Archean continental rocks are composed of Archean TTG series that formed during subduction by partial melting of hydrated oceanic crust transformed into garnet amphibolite or eclogite, geochemically similar to modern 'adakites' proposed by Defant and Drummond (1990). Therefore, the role of high-Mg andesitic magma in the continental crust growth is greatly discussed (*e.g.*, Kawabata and Shuto, 2005; Qian and Hermann, 2010; Tsuchiya et al., 2005) and the relations with associated medium- to low-Mg igneous rocks remain to be resolved.

The HMA magmas solidify as high-Mg diorites when they intrude into lower to middle crust. However, not all of high-Mg diorites are necessarily solidified from HMA magmas because their intrusive feature suggests alternatively the possibility of the mafic cumulates solidified from a different magma to the HMAs. The primary high-Mg diorites have the same geological implications as the HMAs and need to be confirmed by coupled geochemical indicators of whole rock compositions and mineral chemistry (Kamei et al., 2004). Besides the Late Archean times, high-Mg diorites have been widely observed in the Cenozoic and Mesozoic blocks/cratons and their petrogenesis has been discussed in terms of four main models: (1) partial melting of enriched mantle (Tatsumi, 1982; Tatsumi and Ishizaka, 1981), (2) interaction of subducting slab-derived adakitic melts and mantle wedge (Tatsumi et al., 2006; Tsuchiya et al., 2005), (3) partial melting of delaminated thickened lower crust (Gao et al., 2004; Moyen et al., 2003; Rapp et al., 2010; Xu et al., 2010; Yogodzinski et al., 1995), and (4) interaction of felsic magmas with ultramafic rocks at crustal level (Qian and Hermann, 2010). In contrary to the huge documentation on Cenozoic HMA and their Archean analogues, rare Neoproterozoic high-Mg diorites have been investigated (*e.g.*, Zhao et al., 2010) and the subducting slabs at the time are commonly considered not very hot. More studies for the high-Mg diorites of that period will shed light on the petrogenesis of HMAs and continental crust growth.

In this work, we gave a synthetic geochemical study on the Neoproterozoic (ca. 830 Ma) high-Mg diorites in the western part of the Jiangnan orogen (Wang et al., 2007; Zhou et al., 2009) that separates the Yangtze Block from the Cathaysia (Fig. 1a). A petrogenetic link between the diorites and the associated medium- to low-Mg granodiorites is investigated and their tectonic implications for the Neoproterozoic subduction in the western part of the Jiangnan orogen are also discussed.

2. Geological background

The nearly W-E-trending Jiangnan orogen divides the South China Block (*i.e.*, southern China) into the Yangtze Block to the northwest and the Cathaysia Block to the southeast (Fig. 1a). It is composed mainly of Neoproterozoic igneous (ca. 960–750 Ma) and sedimentary (ca. 860–750 Ma) rocks (including the 'basement sequences' and the 'overlying sequences') metamorphosed to low-greenschist facies (Wang et al., 2014). The orogenic belt can be divided into two parts (eastern and western). The crust in the eastern segment is characterized by depleted Nd and Hf isotopes, while the western part is featured by enriched isotopic compositions (Wang et al., 2014). The ca. 960–860 Ma arc volcanic rocks and associated ophiolites were only found in the eastern part and the Neoproterozoic magmatism in the western part formed at ca. 830–800 Ma (Li et al., 2003a,b; Wang et al., 2006; Zhou et al., 2009) and 770–750 Ma (Wang et al., 2008; Zhou et al., 2007). The northern Guangxi Province is just located at the westernmost end of the Jiangnan orogen and consists of most Neoproterozoic igneous rocks in the western part of the Jiangnan orogen.

In the Baotan area of northern Guangxi (Fig. 1b), calc-alkaline mafic rocks are coeval with peraluminous (aluminum saturation index > 1.1) granitic rocks, with an age peak of ca. 820 Ma (Li et al., 2003b; Wang et al., 2006; Zhou et al., 2004). The granitic rock is the dominant rock type and can be divided into two main groups: coarse-grained biotite granite and medium- to fine- grained granodiorite (Ge et al., 2001a; Qiu et al., 2002; Wang et al., 2006). The biotite granites intruded the granodiorites although their zircon U-Pb ages may be indistinguishable within analytical errors. This intrusive relationship is evident at the contact zone between the Sanfang Pluton (biotite granite) and the Bendong Pluton (granodiorite) as seen in the field sketch Fig. 2 of Wang et al. (2006).

The Dongma Pluton intrudes the slate and phyllite of the 'basement sequences' (*i.e.*, the Sibao Group) in the study area. It is just in contact with the southernmost margin of the Bendong Pluton (Fig. 1c) but the contact zone is not clear due to the poor outcrop. Wang et al. (1982) considered the Dongma Pluton as a composite composed of some intrusions to the south of the Bendong Pluton, associated with some hornblendites that intruded into the Sibao Group. The main rock types of the Dongma Pluton are granodiorite and tonalite. The tonalite (*i.e.*, the high-Mg diorites of this study) is distributed at the southern part of the Dongma Pluton (Fig. 1c) and sporadic major element analyses of the high-Mg diorites have been shown in the published references (Sun, 1982; Wang et al., 1982, 2006; Zhao et al., 1987). Recent *in situ* U-Pb zircon dating suggested that the diorites formed at 837 ± 7 Ma (Wang et al., 2014), consistent with the ages of other Neoproterozoic granodiorites in the area.

3. Analytical methods

Electronic microscope composition and Backscatter Electron (BSE) images were obtained with a JEOL JXA-8230 electron microprobe at The Analytical Center of Shandong Bureau of China Metallurgy and Geology. The analyses were performed under an accelerating voltage of 15 kV and an electric beam of 10 nA focusing on a spot of 5 μm in diameter (1 μm for smaller minerals). Analytical precisions of the analyses are better than 0.1 wt%. The Fe^{3+} concentrations were calculated in accordance with spinel stoichiometry.

The samples were powered carefully to make grain size less than 200 meshes (equal to 74 μm) and then are ready for analyzing. Whole-rock major elements were analyzed using a Thermo Scientific ARL 9900 X-ray fluorescence spectrometer (XRF) at the State Key Laboratory for Mineral Deposits Research (MiDeR), Nanjing University (NJU). The analytical precision is generally less than 2%. Whole-rock rare earth and other trace elements were analyzed using an ICP-MS (Finnigan MAT-Element II) instrument at MiDeR-NJU. Each sample was precisely weighted 30 mg and then was put into a 15 ml Savillex digestion vessel. After being dissolved by HNO_3 and the injection of 1 ml 500 ng/ml internal standard Rh solutions, the samples are ready for analyzing. Analytical precision for most elements by ICP-MS is better than 5%.

The Sr-Nd-Hf isotopes were determined using a Neptune (plus) MC-ICP-MS (Finnigan MAT Triton TI) at MiDeR-NJU, following the methods similar to Chu et al. (2009) and Yang et al. (2010). For Sr-Nd isotopes,

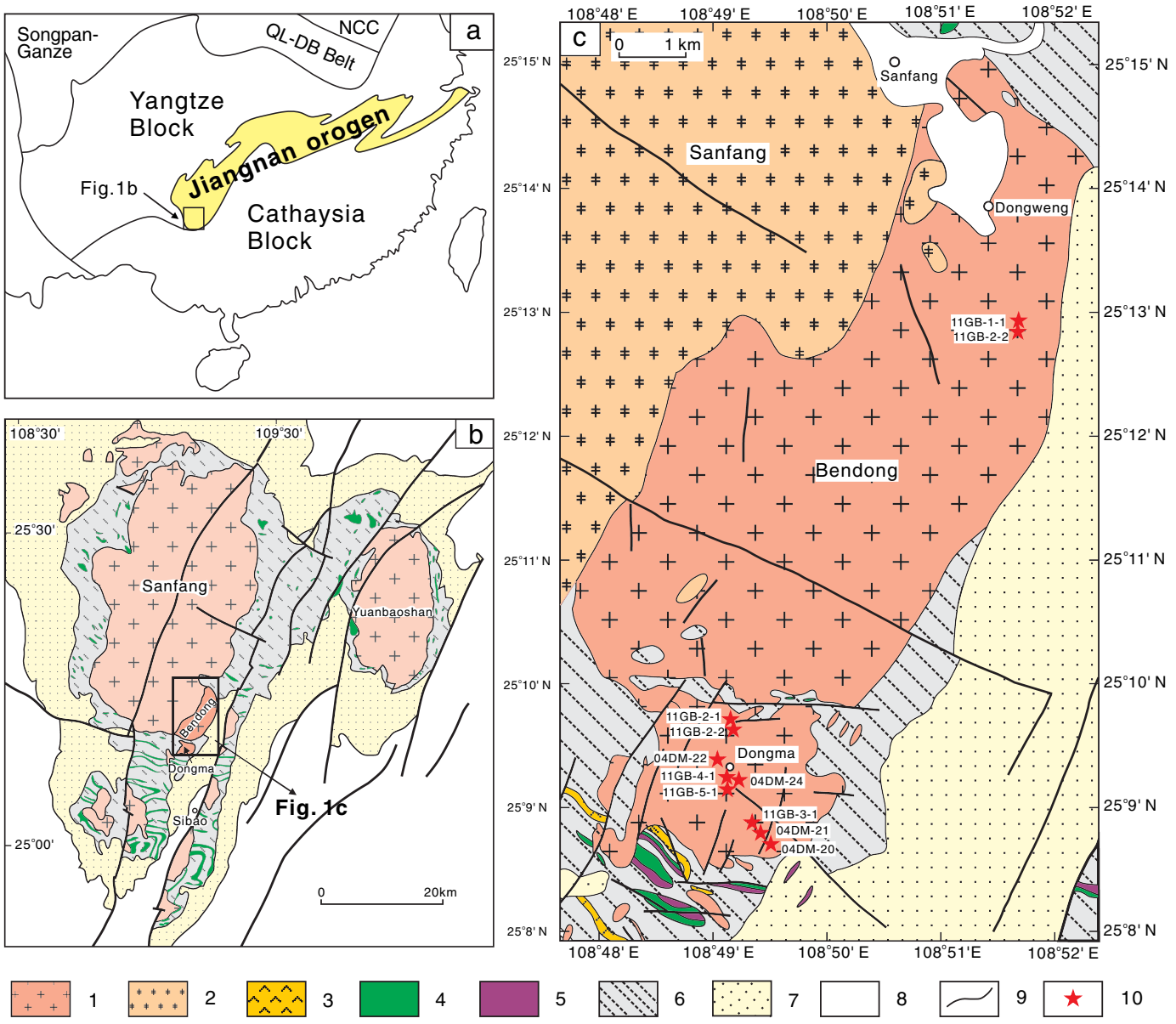

Fig. 1. Geological map of (a) southern China Block; (b) Bendong and Dongma plutons (modified after GXRGST, 1987, 1995). NCC, North China Craton; QL-DB belt, Qinling-Dabie belt. 1, first-stage diorites and granodiorites; 2, second-stage biotite granites; 3, Neoproterozoic mafic volcanic rocks; 4, Neoproterozoic mafic rocks; 5, Neoproterozoic ultramafic rocks; 6, Neoproterozoic Sibao Group; 7, Neoproterozoic Danzhou Group; 8, Sinian to Quaternary system; 9, faults; 10, sampling location.

about 50–100 mg of powdered sample was dissolved and purified. NIST SRM-987 and JNdi-1-Nd were used as reference standards, yielding average $^{87}Sr/^{86}Sr$ ratio of 0.710251 ± 13 (n = 4, 2sd) and $^{143}Nd/^{144}Nd$ ratio of 0.512106 ± 0.000016 (n = 3, 2 sd), identical to certified value of 0.71034 ± 0.00026 (NIST certificate) and in agreement with the commonly accepted value of 0.71025 ± 0.00026 (*e.g.*, Nyquist et al., 1994; Stein et al., 1997). The εNd(t) values were calculated based on the Nd isotopic compositions of $^{143}Nd/^{144}Nd$ (CHUR) = 0.512638 and $^{147}Sm/^{144}Nd$ (CHUR) = 0.1966 for CHUR (Carlson et al., 2007; Hamilton et al., 1983; Jacobsen and Wasserburg, 1984). For the Hf isotope analyses, about 50 mg of powdered sample was placed in a stainless lined PTFE bomb, and 1 ml of HF and 1 ml of HNO_3 were added to dissolve the samples. 500 ng of Re was added as an internal standard. 0.4 mL of 3 mol/L of HCl was pipetted into a 15 ml centrifuge tube and make up to 8 ml for measuring the concentration of Lu (^{175}Lu) and Hf (^{178}Hf) by ICP-MS using Re as internal standard. The remnant solution was loaded onto a pre-conditioned 0.5 mL Ln Spec resin column. The matrix elements (including Ti) and Rare Earth Elements (including Lu and Yb) were eluted with 20 ml of 6 M HCl + 0.5% H_2O_2. Finally, Hf (+Zr) was extracted from the column with 5 mL of 2 M HF and collected in a 10 mL PFA beaker. The solution was gently evaporated to dryness and dissolved with 1 ml of 5% HNO_3. The average value of the standard JMC-475 is 0.282159 ± 14 (n = 7, 2sd).

4. Petrography and Mineralogy

The high-Mg diorites are fine-grained with plagioclase, biotite and quartz as the dominant minerals (Table 1). Plagioclase is mainly replaced by sericite, and biotite is replaced by chlorite with Fe-oxide precipitation within the biotite (Fig. 2a). The medium-Mg granodiorites have similar mineral assemblage (Table 1) and alterations in minerals (*e.g.*, plagioclase and biotite), but the quartz minerals are relatively big (versus the recrystallization of quartz in the high-Mg diorites) in size

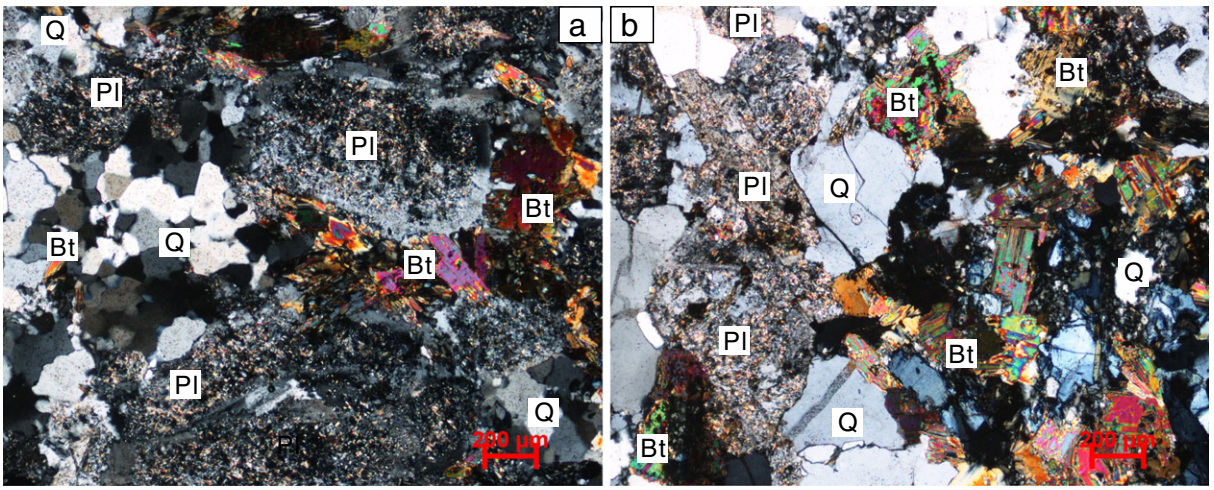

Fig. 2. Micro-images for representative high-Mg diorites from the Dongma Pluton (a) and medium-Mg granodiorites from the Dongma Pluton (b). Q–quartz, Bt–biotite, Chl–chlorite, Pl–plagioclase.

(Fig. 2b). The electron microscope analyses for representative minerals are shown in Table S1–2 in Appendix.

4.1. Plagioclase

Plagioclase crystals in the studied three types of rocks are mostly altered. Some of them were transformed to albite and are spatially associated with other secondary minerals (*e.g.*, ilmenite, chlorite, sericite). The altered plagioclases have decreased CaO (0.2–1.8 wt%) and elevated FeO (0.08–0.37 wt%) and Na_2O (7.7–10.7 wt%) contents relatively to the primary plagioclase (Table S1). In contrast, fresh plagioclase domains mostly show CaO of 3.1–5.7 wt%, yielding anorthite (An) composition ranging 15 to 28, indicating oligoclase in the fresh diorite and granodiorite rocks. One analysis from the core of one plagioclase gave An of 62 (Table S1), indicating normal zonings in the mineral.

4.2. Biotite

Biotite in the high-Mg diorites is mostly altered to secondary chlorite, in which MgO contents are up to 22 wt%. However, the secondary chlorite in the medium-Mg granodiorites has relatively low MgO contents (5.9–6.7 wt%). They have high Al_2O_3 (30.7–32.6 wt%) and low FeO (1.5–2.6 wt%) and MgO (1.5–2.2 wt%) contents, yielding Fe-numbers ($[100 \times Fe^{2+}/(Fe^{2+} + Mg^{2+})]$) of 29–42 (Table S1). No biotites from low-Mg granodiorites were analyzed.

4.3. Fe-oxides

Ilmenite is the dominant opaque Fe-oxides that are commonly associated with chlorite and other secondary minerals. The analyzed ilmenites from the high-Mg diorites and medium-Mg granodiorites show TiO_2 of 47.9–52.9 wt% and total FeO of 40.7–47.9 wt% (Table S1). They also have minor MnO (1.2–4.3 wt%) and MgO (0.02–1.2 wt%). Some ilmenite minerals are surrounded by or associated with perovskite (Fig. 3a, b) which does not generally occur in diorite and granodiorite. The SEM images suggest the perovskites are not euhedral, but as the surroundings of the ilmenite, or as patches within the ilmenite crystals (Fig. 3a, b), indicating the formation by alteration. No magnetites were observed during the study, suggesting theses diorites and granodiorites are similar to typical ilmenite-type granitoids.

4.4. Chromite

Chromite minerals were separated by heavy-liquid and hand-picking from the high-Mg diorites and some of the medium-Mg granodiorites. They are mostly simple in crystal texture under BSE images (Fig. 3c, d). One chromite mineral includes a tiny inclusion composed of quartz + apatite (Fig. 3d). There are no significant chemical variations between the chromites from the two different rock types. The chromites can be divided into two groups according to their TiO_2 concentrations. Relative to the low- TiO_2 ($TiO_2 > 1.0$ wt%) chromites, the high-TiO_2 ($TiO_2 < 0.5$ wt%) chromites have low Al_2O_3 (4.0–7.6 wt% *vs.* 7.7–22 wt%) and high Cr_2O_3 (55.7–62.4 wt% *vs.* 36.0–52.1 wt%). In

Table 1
Percentage (%) of minerals in the studied rocks.

Rock type	Pluton	Sample	Quartz	Feldspar	Biotite	Sericite	Chlorite	Zoisite	Other opaque minerals	Alteration mineral assemblage
High-Mg diorite	Dongma	04-DM-20	20	50	15	4	10	0	1	Sericite + Chlorite + Zoisite
High-Mg diorite	Dongma	04-DM-21	25	43	15	10	5	0	2	Sericite + Chlorite + Zoisite
Medium-Mg granodiorite	Dongma	11GB-4-1	35	45	15	0	5	0	0	Sericite + Chlorite + Zoisite
Medium-Mg granodiorite	Dongma	11GB-5-1	35	50	7	0	7	0	1	Sericite + Chlorite + Zoisite
Medium-Mg granodiorite	Dongma	04-DM-22	30	50	12	0	5	1	2	Sericite + Chlorite + Zoisite
Medium-Mg granodiorite	Dongma	04DM-24	30	50	15	0	2	3	0	Sericite + Chlorite + Zoisite
Low-Mg granodiorite	Bendong	11GB-1-1	35	50	5	7	3	0	0	Sericite + Chlorite + Zoisite
Low-Mg granodiorite	Bendong	11GB-1-2	40	35	13	8	1	2	1	Sericite + Chlorite + Zoisite
Low-Mg granodiorite	Bendong	11GB-2-1	25	57	15	1	0	2	0	Sericite + Chlorite + Zoisite
Low-Mg granodiorite	Bendong	11GB-2-2	30	50	13	0	3	4	0	Sericite + Chlorite + Zoisite

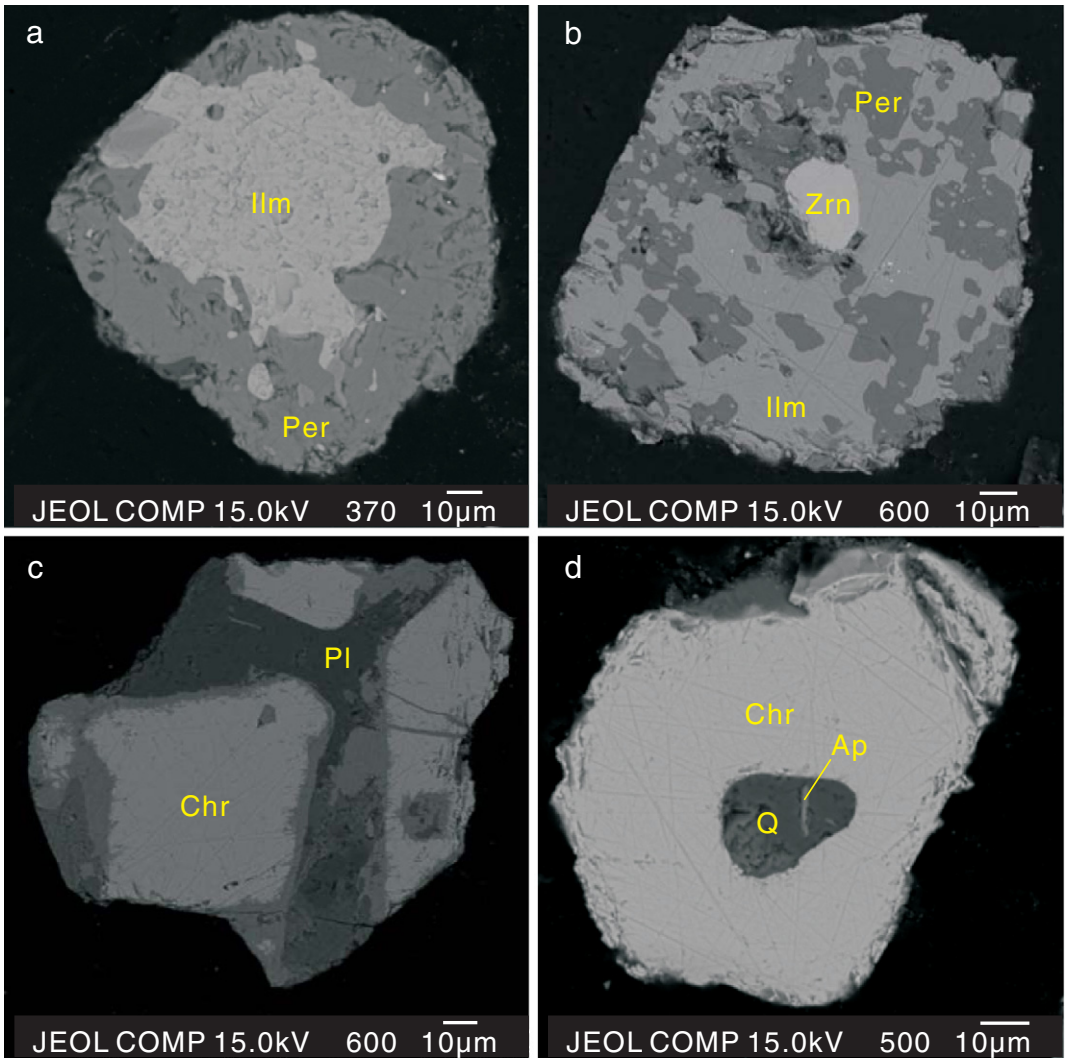

Fig. 3. Backscatter Electron (BSE) images of chromite and ilmenite from medium-Mg granodiorites (a, b, d) and high-Mg diorites (c) in the Dongma Pluton. (a), ilmenite is surrounded by perovskite; (b), one tiny zircon grain was found in the middle of an ilmenite that was partly replaced by perovskite; (c), one chromite mineral is associated with plagioclase; (d) apatite + quartz composite was found within a chromite, indicating the formation of felsic magmas before the crystallization of the chromite. Ilm–ilmenite, Per–perovskite, Zrn–zircon, Chr–chromite, Pl–plagioclase, Ap–apatite.

addition, the high TiO_2 chromites tend to have low FeO and ZnO and high MgO. All the chromite minerals have high Cr-number (Cr# = 50–85, average of 75) but low Mg-number ($100 \times Mg^{2+} / (Mg^{2+} + Fe^{2+})$) (Mg# = 0.3–2.5) (Table S2).

5. Whole-rock geochemistry

5.1. Major elements

The studied rocks can be divided into three groups according to their sampling localities and whole-rock geochemistry (Table 2; Fig. 4). Group-1 is the high-Mg diorites (MgO = 6.7–8.9 wt%) and they are from the southern part of the Dongma Pluton; group-2 is the medium-Mg granodiorites (MgO = 3.4–3.8 wt%) from the Dongma main body; and group-3 is the low-Mg granodiorites (MgO = 1.4–1.9 wt%) from the Bendong Pluton.

The high-Mg diorites show lowest SiO_2 (59–65 wt%), FeO*/MgO, Al_2O_3 and K_2O (1.6–3.3 wt%) (Table 2; Fig. 4). They are characterized by high MgO (6.7–8.9 wt%) concentrations and Mg-number (69–73) (Table 2). Their TiO_2 concentrations (0.43–0.56 wt%) are higher than those of boninites and other group rocks. The high-Mg diorites are peraluminous in geochemistry, with aluminum saturation index (ASI = molarAl_2O_3/molar(CaO + Na_2O + K_2O)) of 1.4–2.2 (except one sample at 1.04) (Table 2), which may resulted from the Ca mobility during alteration.

The medium- and low-Mg granodiorites have elevated SiO_2 (65–69 wt%), Al_2O_3 (14.5–15.9 wt%) and K_2O (mostly of 2.6–4.0 wt%) (Table 2; Fig. 4). The MgO contents of the medium-Mg granodiorites range from 3.4 to 3.8 wt%, while the low-Mg rocks show MgO of 1.4–1.9 wt% (Table 2). Correspondingly, they have high FeO*/MgO ratios (1.03–2.07, versus 0.14–0.75 of the high-Mg diorites) and low Mg# (46–63). These rocks are also strongly peraluminous (ASI = 1.2–1.7) (Table 2).

5.2. Trace elements

The high-Mg diorites are characterized by high Cr (595–640 ppm) and Ni (171–194 ppm) concentrations. Along with the increasing of SiO_2 contents, the Cr and Ni concentrations decrease from the medium-Mg Dongma granodiorites to the low-Mg Bendong granodiorites (204–348 ppm versus 43–61 ppm, and 47–99 ppm versus 15–18 ppm) (Table 2; Fig. 4). The other difference between the high-Mg diorites and the medium- to low-Mg granodiorites is their relatively small negative Eu anomalies (average of 0.74 versus 0.64; Fig. 5a, b) and

Table 2
Major element contents (wt%) and trace element concentrations (ppm) in samples from the Dongma and Bendong plutons.

No.	1	2	3	4	5	6	7	8	9	10	11	12	13
Pluton	Dongma	Dongma	Dongma	Dongma	Dongma	Dongma	Dongma	Dongma	Dongma	Bendong	Bendong	Bendong	Bendong
Rock type	High-Mg diorites					Medium-Mg granodiorites				Low-Mg graodiorites			
Sample	10GB3-1	04DM-20	04DM-21	G-15[1]	B57-1[2]	11GB4-1	11GB5-1	04DM-22[3]	04DM-24	11GB1-1	11GB1-2	11GB2-1	11GB2-2
SiO_2	61.90	60.84	59.21	62.08	65.05	64.99	65.76	66.55	64.75	68.75	68.19	67.61	67.5
TiO_2	0.48	0.56	0.54	0.46	0.43	0.44	0.44	0.46	0.43	0.32	0.37	0.39	0.36
Al_2O_3	13.33	13.3	13.76	12.93	12.59	15.88	15.3	15.49	15.21	15.36	14.55	15.01	15.24
$Fe_2O_3^t$	5.99	7.08	7.13	1.38	1.04	4.36	4.27	4.73	4.54	3.1	3.61	3.64	3.44
FeO				4.54	4.43								
MnO	0.12	0.12	0.14	0.13	0.08	0.08	0.07	0.08	0.11	0.07	0.08	0.07	0.07
MgO	8.29	8.5	8.92	7.63	6.65	3.8	3.43	3.37	3.5	1.35	1.84	1.94	1.56
CaO	0.76	1.23	1.93	2.74	2.13	1.08	1.35	2.73	2.19	1.54	1.19	1.62	2.2
Na_2O	1.48	2.1	1.05	2.38	1.75	2.22	3.24	2.75	2.58	2.88	2.73	2.5	2.9
K_2O	2.02	1.55	1.97	3.26	2.24	3.3	2.68	1.94	3.01	3.97	3.99	3.86	3.7
P_2O_5	0.06	0.1	0.1	0.13	0.08	0.08	0.09	0.13	0.12	0.16	0.14	0.1	0.11
LOI	4.50	4.88	5.06	2.95	3.41	4.51	2.27	1.66	2.14	1.64	1.9	2.07	1.83
SUM	98.93	100.26	99.81	100.6	99.88	100.73	98.89	99.89	98.64	99.14	98.59	98.82	98.92
ASI[4]	2.22	1.8	1.87	1.04	1.37	1.73	1.43	1.34	1.32	1.3	1.32	1.34	1.19
$Na_2O + K_2O$	3.50	3.66	3.02	5.64	3.99	5.51	5.92	4.69	5.59	6.85	6.72	6.36	6.60
FeO^*/MgO[5]	0.65	0.75	0.72	0.16	0.14	1.03	1.12	1.26	1.17	2.07	1.77	1.69	1.98
Al_2O_3/TiO_2	27.5	23.7	25.5	28.1	29.3	35.8	35.2	33.7	35.4	48.1	38.8	38.1	42.3
Mg#[6]	73	70	71	70	69	63	61	59	60	46	50	51	47
Li	75.7	60.4	87.1			48.2	44.1	27.9	48.0	39.3	53.3	35.2	29.7
Be	1.74	1.64	1.16			2.31	1.85	0.98	2.06	1.85	1.64	1.94	2.09
Sc	16.8	15.9	16.4			14.0	12.6	10.5	5.56	10.8	12.8	12.7	11.8
V	68.8	113	22.6			34.7	33.9	42.8	24.3	34.4	40.3	40.0	40.1
Cr	629	640	595			241	204	343	348	46.3	61.5	51.6	43.3
Co	24.6	29.1	32.5			12.5	10.3	15.8	15.8	7.51	8.50	7.61	7.08
Ni	170	187	194			51.1	47.2	59.6	98.8	15.3	18.4	16.8	15.1
Cu	20.5	30.0	21.8			5.58	6.96		6.44	104	89.9	8.17	6.74
Zn	79.7	119	81.4			66.0	66.5	101	104	49.0	59.9	82.7	65.7
Ga	18.3	17.0	16.5			22.5	21.0	19.2	13.0	20.6	20.7	19.5	20.9
Rb	123	105	121			179	128	83.5	24.1	217	235	182	172
Sr	70.8	99.5	88.2			165	167	217	32.8	138	133	140	150
Y	22.6	37.7	42.2			20.5	21.5	22.1	13.3	22.5	22.4	24.4	24.5
Zr	155	175	132			211	191	200	186	148	152	192	178
Nb	6.57	6.83	6.15			9.98	9.49	9.87	9.97	10.2	11.7	11.1	10.6
Mo	0.63	0.41	0.29			0.47	0.62		0.61	7.6	2.75	0.20	0.21
Cd	0.26	0.16				0.27	0.24			0.25	0.18	0.22	0.30
Sn	2.14	1.87	1.85			2.74	2.62	6.63	1.08	11.7	5.31	8.76	7.20
Cs	7.66	7.22	9.80			7.40	5.74	6.47	5.78	16.2	18.1	6.59	6.21
Ba	385	225	375			522	371	383	106	339	377	542	497
La	18.9	28.0	25.6	20.5		32.3	31.7	32.6	14.8	23.9	26.4	35.5	32.9
Ce	38.2	48.3	50.9	42.3		67.7	59.8	53.7	23.6	54.4	57.9	76.6	73.5
Pr	4.35	6.78	6.57	7.28		7.71	6.99	6.42	5.10	5.6	5.88	7.73	7.41
Nd	17.5	27.5	26.1	17.5		30.2	27.2	26.0	19.4	21.7	23.1	30.3	29.3
Sm	3.62	5.91	5.89	4.14		5.39	5.11	5.48	3.95	4.31	4.37	6.19	5.66
Eu	0.87	1.28	1.66	0.85		0.95	1.01	1.16	0.78	0.9	0.86	1.17	1.20
Gd	3.55	5.99	5.86	2.95		4.72	4.42	3.95	3.51	3.82	3.96	5.25	5.05
Tb	0.51	0.88	1.16	0.79		0.64	0.62	0.64	0.57	0.58	0.59	0.72	0.67
Dy	3.76	5.97	7.48	2.27		4.23	4.02	3.62	3.19	3.66	3.99	4.80	4.27
Ho	0.83	1.38	1.52	0.62		0.78	0.86	0.82	0.59	0.78	0.79	0.95	0.96
Er	2.49	3.92	4.20	1.75		2.51	2.47	2.14	1.73	2.4	2.51	2.84	2.94
Tm	0.37	0.53	0.64	0.29		0.35	0.35	0.35	0.24	0.33	0.39	0.41	0.40
Yb	2.22	3.37	3.79	2.72		2.27	2.20	2.07	1.57	2.09	2.39	2.43	2.53
Lu	0.35	0.57	0.63	0.25		0.33	0.32	0.36	0.24	0.3	0.35	0.35	0.37
Hf	4.10	4.83	3.57			5.45	4.87	5.80	5.45	4	3.94	4.88	5.16
Ta	0.55	0.56	0.56			0.77	0.72	0.90	0.58	1.1	1.25	1.00	1.25
W	1.40	1.12	1.63			2.07	1.79	1.30	1.08	14.6	4.84	1.60	1.77
Pb	10.4	5.51	14.1			13.6	12.6	26.0	18.9	15.5	20.3	22.0	25.0
Bi	0.05	0.08	0.11			0.11	0.12	0.18	0.08	0.98	4.24	0.24	0.25
Th	6.42	8.22	7.02			10.3	9.90	12.7	6.16	8.31	8.82	12.0	12.1
U	1.29	1.42	1.41			2.21	1.94	2.27	1.07	3.11	3.64	2.63	2.60

[1] Zhao et al. (1987); $Fe_2O_3^t$ of this sample is just Fe_2O_3.
[2] Sun (1982); $Fe_2O_3^t$ of this sample is just Fe_2O_3.
[3] Wang et al. (2006).
[4] ASI = molarAl_2O_3 / molar(CaO + Na_2O + K_2O).
[5] FeO* is the total ion shown as FeO.
[6] Mg# = $(Mg^{2+}/(Mg^{2+}+Fe^{2+}))$*100.

low $(La/Yb)_N$ ratios (4.9–6.1 versus 6.8–11.3; Table 2; Fig. 5a, b). The other incompatible elements show similar compositions in all the studied rocks, as indicated by similar normalized REE (Fig. 5a, b) and trace element patterns (Fig. 5c, d). These rocks are enriched in light REE (Fig. 5a, b) and the heavy REE is not low (Yb = 2.2–3.8 ppm for the high-Mg diorites; Table 2). All the samples show strong enrichment in

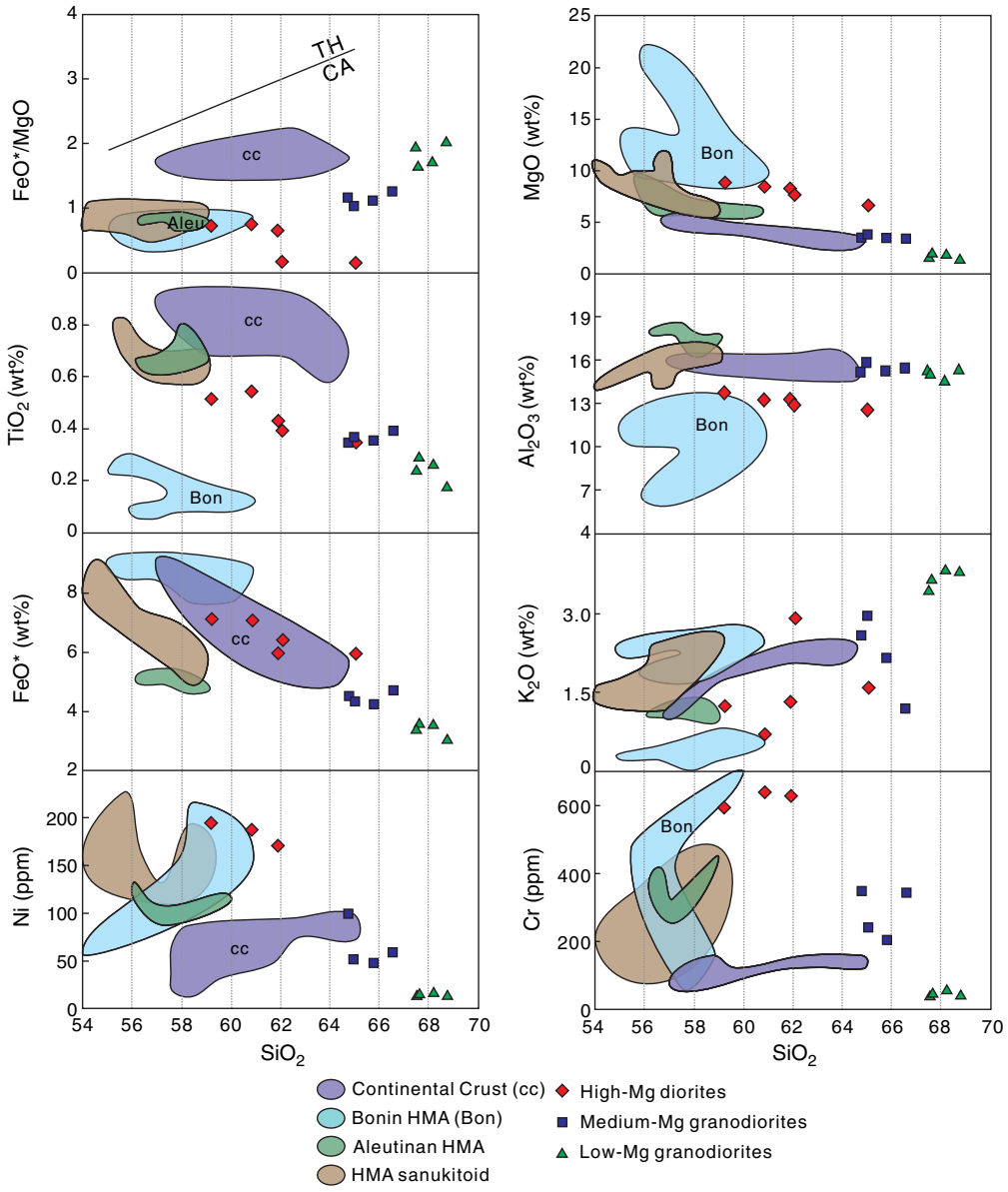

Fig. 4. Harker diagrams showing the variation of major and trace elements versus SiO_2 concentrations.

Pb and depletions in Nb and Ti (Fig. 5c,d). In general, the high-Mg diorites are geochemically similar to the Setouchi HMAs and different from the adakites and Bonin HMAs (Fig. 5c). In addition, the high-Mg diorites show low Sr/Y (2.1–3.1) ratios, which are significantly different from typical adakites and boninites but similar to typical normal arc volcanic rocks (Fig. 6a).

5.3. Sr-Nd-Hf isotopes

The high-Mg diorites and medium- to low-Mg granodiorites show high Rb/Sr ratios (0.77 to 1.77, except one at 0.38; Table 3), but their initial $^{87}Sr/^{86}Sr$ (I_{Sr}) ratios are slightly different. Four samples show I_{Sr} lower than 0.700, which may have been resulted from their high Rb/Sr ratios. The other analyses show large variation of I_{Sr} (0.7028–0.7125; Table 3), which possibly resulted from the alteration and indicates that the Sr isotopes may be not reliable for these analyses.

Nd isotopes also show variations within the three types: the high-Mg diorites show the lowest εNd(t) (−4.9 to −5.4) while the medium- to low-Mg granodiorites tend to show lightly higher εNd(t) (−3.2 to −5.9 and −4.2 to −5.2; Table 3). Hf isotopes show contrasting compositions between the high-Mg diorites and other granodiorites. The high-Mg diorites show lightly higher $^{176}Hf/^{177}Hf$ (0.282440 – 0.282497) and $^{176}Lu/^{177}Hf$ ratios (0.015–0.026), yielding enriched εHf(t) (−6.03 to −6.22, except for 11GB-3-1 at −1.96) (Table 3). However, the medium-Mg granodiorites have $^{176}Hf/^{177}Hf$ ratios of 0.282393–0.282415 and $^{176}Lu/^{177}Hf$ ratios of 0.009–0.011, which yielded relatively depleted εHf(t) values (−1.07 to +0.05) (Table 3).

6. Discussion

6.1. Crustal contamination versus mantle metasomatism

Since Neoproterozoic mafic rocks are developed in northern Guangxi, it is necessary to discuss the possibility of crustal contamination of mantle-derived mafic magma to form the high-Mg diorites. The enriched Nd-Hf isotope characteristics of the high-Mg diorites and associated mafic rocks seem to support the possibility. Similarly, Ge et al. (2001b) suggested that some of the mafic–ultramafic rocks in northern Guangxi have experienced significant crustal contamination. However, it should be noted that the contaminated crust endmember

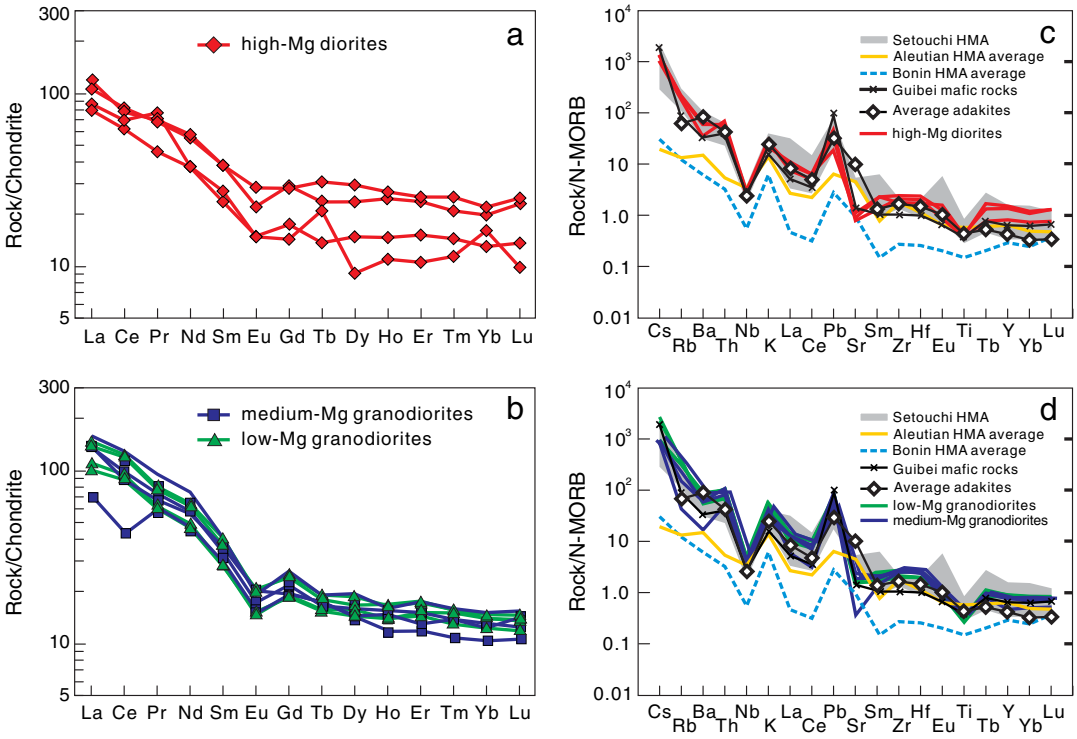

Fig. 5. Chondrite normalized REE patterns and N-MORB normalized trace element patterns for the studied rocks. (a) and (c), high-MgO diorites; (b) and (d), medium- and low-MgO granodiorites. Normalization values are from Sun and McDonough (1989). The average composition of Neoproterozoic mafic rocks in the Baotan area of northern Guangxi is calculated from the data of Zhou et al. (2000, 2004) and Ge et al. (2000).

is yet to be determined. No sedimentary sequences older than the Sibao Group have been found in the western part of the Jiangnan orogen. If we consider the Neoproterozoic granitic rocks as the product of partial melting of lower to middle crust, their source rocks could represent the crust endmember. However, these granitic rocks generally show similar Nd isotope features as the associated mafic rocks. In particular, some mafic rocks even show more enriched Nd isotopes than the high-Mg diorites and the granitic rocks (i.e., lower initial Nd isotope ratios) (Table 3; Fig. 7), which suggest that the source rocks for the granitic rocks are inadequate to be the crustal endmember for contamination. If we adopt the most depleted sample from northern Guangxi (98GX-6-3 from the Yuanbaoshan area; $\varepsilon Nd(t) = 5.24$; Ge et al., 2001b) as the depleted mantle endmember and the average compositions of metasediments of the intruded Sibao Group as the crust endmember, a simple modeling by Nd isotopes and Nd concentrations suggests that the high-Mg diorites can be generated from the 40%–70% crustal contamination of the depleted mantle-derived magmas (Fig. 7). This large proportion of crustal contamination is unlikely to happen. Moreover, the high MgO, Ni and Cr contents are inconsistent with significant crustal contamination. Especially, the MgO contents of the high-Mg diorites are evidently higher than those of the diorites (MgO = 4.5–5.5 wt%; Ge et al., 2000) that formed by fractional crystallization of mafic magmas and are even higher than the values of most mafic rocks in northern Guangxi (Zhou et al., 2004). In addition, if we consider the Hf isotopes, the significant crustal contamination should result in increasing Hf isotopes which, however, are absent in the high-Mg diorites and the associated mafic rocks.

In contrast, we propose the enriched Nd-Hf isotopes of the high-Mg diorites and some of the associated mafic rocks resulted from the metasomatism by the subducting terrigenous sediments. Similar metasomatism has also been found in the Setouchi HMAs in SW Japan (Shimoda and Tatsumi, 1999; Shimoda et al., 2003). The metasomatism by melts from subducting sediments can be evidenced by the Ba/Th versus $(La/Sm)_N$ plot (Fig. 8). It is possible that the subducted sediments are rather

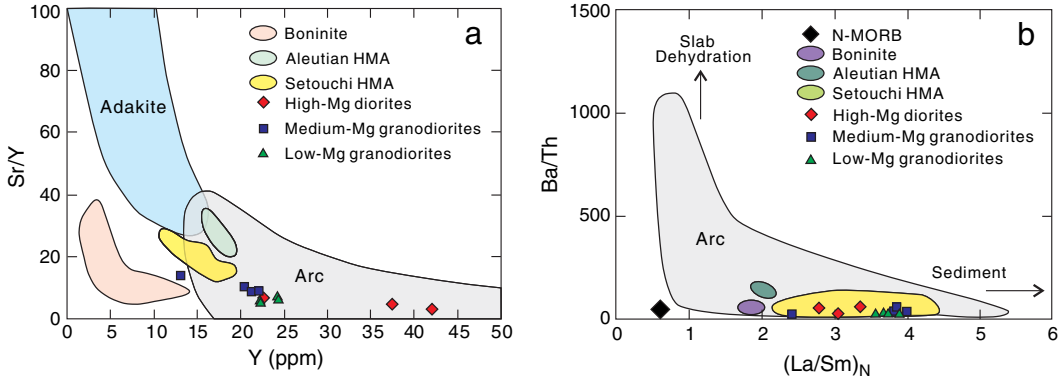

Fig. 6. Sr/Y versu Y (a) and Ba/Th versus $(La/Sm)_N$ (b) plots for the studied rocks in northern Guangxi (after Tatsumi, 2006). Chondrite values for normalization are from Sun and McDonough (1989).

Table 3
Whole-rock Sr-Nd-Hf isotope analyses for the studied rocks from northern Guangxi.

No.	1	2	3	4	5	6	7	8	9	10
Sample	04DM-20[1]	04DM-21	11GB-3-1	04DM-22	11GB4-1	11GB5-1	11GB-1-1[2]	11GB-1-2	11GB-2-1	11GB-2-2
Pluton	Dongma	Dongma	Dongma	Dongma	Dongma	Dongma	Bendong	Bendong	Bendong	Bendong
Rock type	high-Mg diorite	high-Mg diorite	high-Mg diorite	Medium-Mg granodiorite	Medium-Mg granodiorite	Medium-Mg granodiorite	Low-Mg granodiorite	Low-Mg granodiorite	Low-Mg granodiorite	Low-Mg granodiorite
t = Age (Ma)	830	830	830	830	830	830	830	830	830	830
Rb (ppm)	105	121.0	123.2	83.5	179	128	217.1	235.0	182.0	171.8
Sr (ppm)	99.5	88.15	70.77	217	165	167	138.3	133.0	140.0	150.0
Rb/Sr	1.05	1.37	1.74	0.38	1.09	0.77	1.57	1.77	1.30	1.14
$^{87}Rb/^{86}Sr$	3.05	3.97	5.03	1.11	3.14	2.22	4.54	5.11	3.76	3.31
$^{87}Sr/^{86}Sr$	0.74661	0.74256	0.75245	0.72571	0.73586	0.73210	0.76088	0.76811	0.74345	0.74206
±2 SE	0.00008	0.00006	0.00008	0.00010	0.00010	0.00010	0.00004	0.00008	0.00010	0.00008
$(^{87}Sr/^{86}Sr)i$	0.7105	0.6955	0.6928	0.7125	0.6986	0.7058	0.7071	0.7076	0.6989	0.7028
Sm (ppm)	5.91	5.89	3.62	5.48	5.39	5.11	4.31	4.37	6.19	5.66
Nd (ppm)	27.49	26.11	17.49	26.0	30.2	27.2	21.73	23.13	30.31	29.33
$^{147}Sm/^{144}Nd$	0.12998	0.13637	0.12501	0.12748	0.10817	0.11359	0.12003	0.11436	0.12347	0.11669
$^{143}Nd/^{144}Nd$	0.512	0.512059	0.511994	0.511962	0.511992	0.511946	0.511982	0.511978	0.511972	0.511970
±2 SE	6	18	16	32	8	8	12	12	16	10
$(^{143}Nd/^{144}Nd)i$	0.511292	0.511317	0.511314	0.511268	0.511403	0.511328	0.511329	0.511356	0.511300	0.511335
T_{DM}(Nd) (Ma)	2090	2143	1982	2094	1670	1830	1896	1795	1985	1850
T_{DM2}(Nd) (Ma)	1935	1894	1900	1971	1758	1877	1876	1833	1921	1866
εNd (t)	−5.40	−4.90	−4.97	−5.85	−3.22	−4.70	−4.68	−4.15	−5.24	−4.56
±2 SE	0.12	0.36	0.32	0.64	0.16	0.16	0.24	0.24	0.32	0.20
Lu (ppm)	0.503	0.557	0.316	0.274	0.314	0.303				
Hf (ppm)	3.170	2.972	2.930	3.947	4.178	3.783				
$^{176}Lu/^{177}Hf$	0.022	0.026	0.015	0.010	0.011	0.011				
$^{176}Hf/^{177}Hf$	0.022	0.282497	0.282442	0.282415	0.282396	0.282414				
±2 SE	7	6	6	5	8	5				
$(^{176}Hf/^{177}Hf)i$	0.28209	0.28208	0.28220	0.28226	0.28223	0.28224				
εHf(t)	−6.03	−6.22	−1.96	0.05	−1.07	−0.79	−1.8			
±2 SE	0.25	0.21	0.21	0.18	0.28	0.18	0.9			
T_{DM} (Hf) (Ma)	2644	3267	1833	1542	1622	1627				
T_{DM2} (Hf) (Ma)	2097	2109	1840	1713	1783	1766				

[1] The Sm-Nd isotopic data of 04DM-20 is from Wang et al. (2013a).
[2] The εHf(t) was from the average εHf(t) value of magmatic zircons form the Bendong Pluton (Zheng et al., 2007).

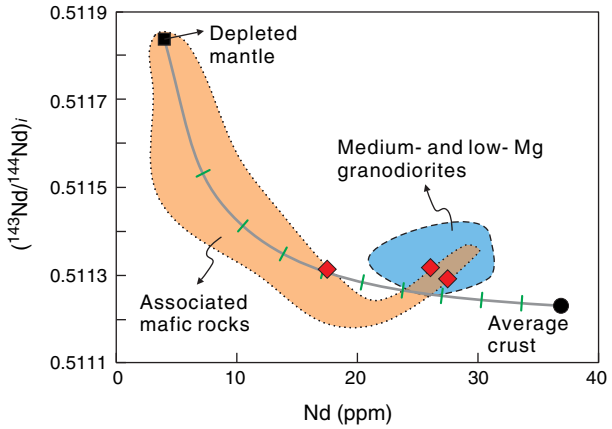

Fig. 7. A simple modeling of crustal contamination of a mantle-derived magma for the formation of high-Mg diorites. A Neoproterozoic peridotite sample (98GX-6-3; Ge et al., 2001b) with most depleted Nd isotopes ($^{143}Nd/^{144}Nd_i = 0.511836$, Nd = 3.96 ppm) in the Yuanbaoshan area of northern Guangxi was selected as mantle endmember. The average composition ($^{143}Nd/^{144}Nd_i = 0.511230$, Nd = 36.94 ppm) of metasediments of the Sibao Group was selected as the crustal endmember for calculation.

old and show enriched isotopes. The variation of Nd isotopes in the Neoproterozoic mafic rocks in northern Guangxi may have been resulted from the heterogeneous metasomatism in the mantle source.

6.2. Formation of the chromites: implications for magma mixing

Chromite [(Fe, Mg)Cr_2O_4] is a common accessory mineral in ultramafic and some mafic rocks (especially ophiolites), and it is very rare in diorites and more felsic rocks because Cr is highly incompatible element, the Cr value in mantle and lower crust is higher than in middle and upper crusts (McDonough and Sun, 1995; Rudnick and Gao, 2004). Even for the formation of differentiated felsic rocks, chromium concentration in the melt will decrease significantly due to the fractionations of early mafic mineral phases (*e.g.*, olivine, pyroxene). Therefore, the chromite minerals in the high-Mg diorites in northern Guangxi are exclusively from mantle-derived melts.

There are two possible mechanisms for the origin of chromites in the high-Mg diorites: (1) they formed directly from primary mantle-derived melts, and (2) they were assimilated from the metasedimentary wall rocks that have received detrital chromites from the exhumation of ultramafic-mafic precursors during the ascending and solidification of felsic magmas. Because the diorites are also characterized by high MgO contents, coupled with the increasing Ni and Cr concentrations, simple crustal contamination could not explain the MgO contents

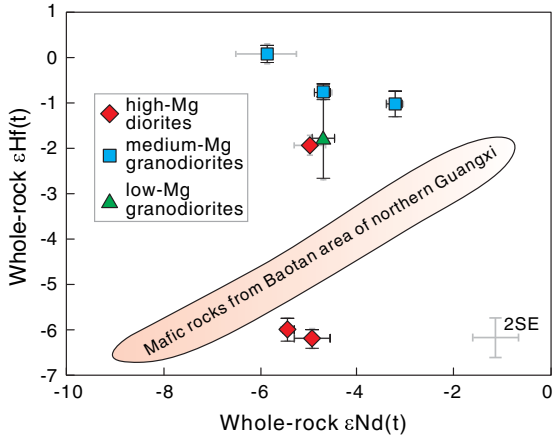

Fig. 8. εHf(t) versus εNd(t) plot for the studied rocks in northern Guangxi. The area of associated mafic rocks was based on our unpublished data.

because the chromite minerals do not have much MgO (Table S2) and no other primary Mg-enriched accessory minerals were found in the rocks. In addition, melting of eclogite, amphibole eclogite or amphibolite source rocks will not produce melts of high Mg# [Mg# > 45] (Rapp et al., 2003). Therefore, only the first mechanism is possible, and the occurrence of chromite minerals suggests the significant contribution of mantle-derived magmas in the formation of high-Mg diorites.

Note the Mg# is decoupled from the Cr# for the chromites. Especially, the Mg# is decoupled from the bulk rock Mg#, which suggests that the chromites are not primary minerals in equilibrium with the high-Mg dioritic magmas. There are two possible explanations for the decoupling: 1) alteration, and 2) diffusion. The alteration of chrome spinel has been investigated about fifty years ago (*e.g.*, Beeson and Jackson, 1969; White, 1966), although this type of mineral is commonly refractory (Barnes and Roeder, 2001). The alteration product is enriched in Fe (sometimes along with Cr) at the expense of Al and Mg, with the transition of chromite to 'ferritchromit' (Beeson and Jackson, 1969). The alteration is commonly accompanied with the replacement of olivine and orthopyroxene by chlorite. However, the studied chromites have consistently low Fe^{3+}/Fe^{2+} ratios, which are unlikely to happen during alteration except the alteration fluids were extremely reductive. Generally, ilmenite tends to have lower Fe^{3+}/Fe^{2+} ratio than chromite. However, the Fe^{3+}/Fe^{2+} ratios of ilmenites which associated with the chromites even show Fe^{3+}/Fe^{2+} ratios comparable to those of the chromites, which preclude the existence of reductive fluids. Different from the alteration process, diffusion can lead to a low Fe^{3+}/Fe^{2+} at a given Fe^{3+} by the increase of Fe^{2+} at the expense of Mg^{2+}. Similar diffusion has been often found at the contact zone between Cr-spinel and other silicate (olivine, orthopyroxene, and clinopyroxene) (Li et al., 1997a). It is possible that the diffusion has taken place within the whole chromite minerals of the studied rocks since we did not find significant core-to-rim variations in compositions. The diffusion, if existed, implies that the primary high-Mg magmas encountered a disequilibrium condition which resulted from the injection of relatively low-Mg magmas. During the magma mixing process, the early mineral phase (probably Cr-spinel and other Mg-enriched minerals) was re-equilibrated with the mixed magmas by the diffusion of Mg. The squeezed Mg has entered into the lattice of chlorite, since its percentages in high-Mg diorites are generally higher than other rocks (Table 1). The quartz + apatite mineral inclusion (Fig. 3d) assemblage within chromite provides another line of evidence for the magma mixing because the two minerals are characteristics of granitic magmas.

6.3. Coupling and decoupling of Nd-Hf isotopes

Note the different geochemical behaviors between Sm-Nd and Lu-Hf isotopic systems. Sm/Nd differentiates a little between different minerals, rock types and crustal reservoirs. However, Lu/Hf varies a lot. That's why sometimes we can see decoupling between Nd and Hf isotopes in some rock types (*e.g.*, Carpentier et al., 2009; Tang et al., 2014; Vervoort et al., 2000; Wu et al., 2006; Zheng et al., 2008). The medium-Mg granodiorites show whole-rock εHf(t) values of −1.07 to +0.05, which are decoupled from whole-rock εNd(t) (−3.2 to −5.9) (Fig. 8). No whole-rock analyses were carried out for the low-Mg granodiorites from the Bendong Pluton, but the magmatic zircons from this type of rocks yielded similar neutral εHf(t) (−1.8 ± 0.9) (Zheng et al., 2007), which is also decoupled from the whole-rock εNd(t) (−4.2 to −5.2). It should be noted that the high SiO_2 contents of the medium- to low-Mg granodiorites are not consistent with an origin from a metasomatized mantle source. Therefore, it is possible that the partial melting of restitic granulite-facies lower crust accounted for the decoupling of Nd-Hf isotopes in the medium- to low- granodiorites. The presence of residual garnet is consistent with the depleted heavy REE (Fig. 5b). However, the depletions are not as significant as typical adakites, indicating the garnet is not a major residue phase in the source.

Among the three analyses of high-Mg diorites, one sample (11GB-3-1) yielded εHf(t) at −2.0, which is very close to the values of medium- to low-Mg granodiorites and is decoupled from its εNd(t) (−5.0). The other two samples show roughly coupled Nd-Hf isotopes, similar to the associated mafic rocks in northern Guangxi (Fig. 8). Different from Nd isotopes that could not change The Hf isotope variation of the high-Mg diorites suggest the changing of melt composition that probably resulted from the mixing of mantle-derived magmas with granitic magmas. The presence of chromites within some of the medium-Mg granodiorites is also the result of magma mixing.

6.4. The high-Mg diorites: a metasomatized mantle origin via mixing with crustal melts

The Cr, Al and Ti compositions of the chromites from the high-Mg diorites are similar to the spinels from island-arc basalts and boninites and are different from the spinels from intra-plate and mid-ocean ridge settings (Fig. 9). As indicated above, the high-Mg diorites from northern Guangxi are geochemically (*i.e.*, similar incompatible element patterns, high MgO, Ni and Cr contents, low Sr/Y and La/Yb ratios) similar to the Setouchi sanukitoids in SW Japan, despite their relatively high Y contents that may result from the lack of garnet as the residual phase. As for the petrogenesis of the sanukitoids, some workers considered as the partial melt of a metasomatized mantle source, while others favored an interaction between mantle and melt from subducting slab or delaminated lower crust (see Tatsumi, 2006; Yin et al., 2010 and references therein). In either hypothesis, a metasomatized mantle source is required.

The experimental data demonstrate that the addition of H_2O alone cannot explain the increases in both SiO_2 and MgO contents (on an anhydrous basis) required to shift from basaltic to (high-Mg) andesitic melts in equilibrium with lherzolite residue (Wood and Turner, 2009). Many researchers have favored a mechanism for high-Mg andesitic (HMA) magma production that involves partial melting of the subducting lithosphere and interaction of these slab-derived, hydrous, silicic melts with the overlying mantle wedge peridotite, as originally proposed by Kay (1978). The partial melting of subducted oceanic crust or thickened mafic continental lower crust and the possible following interaction with mantle peridotite cannot be employed to explain the origins of the high-Mg diorites in northern Guangxi, because their relatively low Sr/Y and La/Yb ratios (Fig. 6a; Table 2) preclude the sources of eclogite or garnet-bearing amphibolite. On the other hand, their high HREE contents are in disequilibrium with great amount of residual garnet during partial melting. This precludes the role of direct oceanic crust derived melt in their genesis (Shimoda and Tatsumi, 1999; Shimoda et al., 1998, 2003). In agreement with experimental results, the geochemical features of the high-Mg diorites are best explained by a low degree of partial melting of refractory mantle (harzburgite) that has been fluxed by slab-derived hydrous melts/fluids. This is in agreement with the model proposed by Shirey and Hanson (1984) for the origin of high-Mg diorites from the Superior Province and consistent with the high pressure melting experiments (Wood and Turner, 2009).

The subduction component, which metasomatizes the original mantle wedge to form the characteristic arc magma sources, can be derived from at least two chemically different slab materials: basaltic altered oceanic crust and more silicic sediments (Tatsumi, 2006). The relative contribution of these two components to magma generation may be identified by using abundances of and/or ratios between particular elements. Fig. 6b suggests that the sediment-derived component, rather than the oceanic crust-derived component, is the major metasomatic agent for the high-Mg diorite magma generation. This is consistent with the high ^{18}O observed in igneous zircons ($\delta^{18}O_{zircon} = 8.44$) from the high-Mg diorites (Wang et al., 2013a) although these zircons can be alternatively explained by the mixing with crust-derived granitic magmas. The incorporation of subducting sediment-derived melts had a high whole-rock $\delta^{18}O$ values and the exchange with the mantle peridotite may have changed significantly the oxygen isotope compositions of the generated andesitic melts.

We propose therefore, that formation of the high-Mg diorites from northern Guangxi followed a subduction where the subducted sediments of the oceanic crust melted and metasomatized the overlying mantle wedge. The associated fluids triggered partial melting of refractory mantle (harzburgite) which generated the parental magma of the HMA (high contents of MgO, Cr, Ni and HREE leading to low ratios of La/Yb). In the same time, the underplated mafic magma heated the middle to lower continental crust, leading to the granitic melts. These mafic magmas ascended and mixed with some of the granitic melts (*i.e.*, the medium- to low-Mg granodiorite melts), generating a disequilibrium for the primary spinels with surrounding granitic melts that facilitated the Mg-Fe exchange as recorded in the chromites from the rocks.

6.5. Implications for the assembly between the Yangtze and Cathaysia blocks

The assembly of the Yangtze and Cathaysia blocks has been one of the key issues in the reconstruction of supercontinent Rodinia (see Zhao and Cawood, 2012 and references therein). The Jiangnan orogen connected the two blocks and undoubtedly played an important role

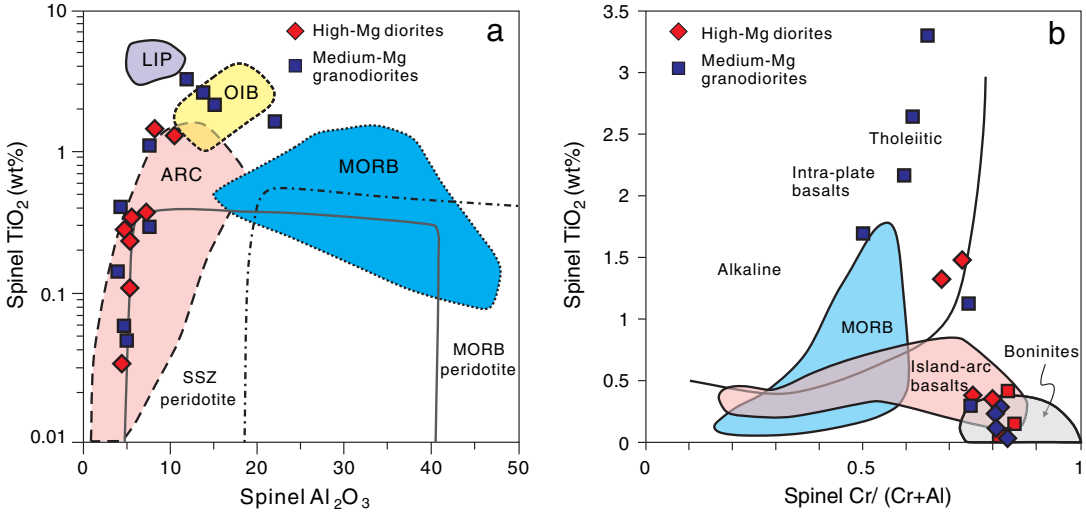

Fig. 9. (a) Al-Ti (Kamenetsky et al., 2001) and (b) Cr#-Ti (after Arai, 1992) plots for chromites in northern Guangxi. LIP, large igneous province; OIB, ocean island basalt; ARC, arc volcanic rocks; MORB, mid-ocean ridge basalt; SSZ, supracrustal subduction zone.

in understanding the amalgamation processes (*e.g.*, Wang et al., 2007). Although there are some different models (*e.g.*, "plate-rift", "slab-arc", "plume") for the Neoproterozoic tectonic evolution of the Jiangnan orogen (*e.g.*, Li et al., 2003a,b, 2009; Wang et al., 2004a, 2004b, 2006; Wu et al., 2006; Zheng et al., 2008; Zhou et al., 2004, 2009), there is a consensus on the oceanic crust subduction at the Early Neoproterozoic despite of that the termination time of subduction is greatly debated. The definite subduction-related arc volcanic rocks are believed to have occurred in the eastern part of the Jiangnan orogen, as represented by the 965–855 Ma Shuangxiwu arc-related rocks in the northwestern Zhejiang Province (*e.g.*, Li et al., 2009; Wang et al., 2007, 2013b; Zheng et al., 2008) and supported by the ophiolites in southern Anhui Province and northeastern Jiangxi Province (*e.g.*, Li et al., 1997b; Zhang et al., 2012a).

The tectonic settings of ca. 830–800 Ma Neoproterozoic igneous rocks in the western part of the Jiangnan orogen were greatly debated. Some scholars suggested that they represented the arc-related and post-collisional magmatic activities (Wang et al., 2006; Zhou et al., 2004, 2009), while other scholars interpreted them as the product of initiation of the ascending of a (super-) plume that finally led to the breakup of supercontinent Rodinia (Li et al., 2003a,b). If the latter tectonic setting were true, the Neoproterozoic subduction at the western part of the Jiangnan orogen would be questionable. The controversy resulted mainly from the different interpretations (*i.e.*, island arcs versus crustal contamination) on the arc-like geochemical features of the mafic–ultramafic rocks in northern Guangxi (Li et al., 2004; Zhou et al., 2004). The discovery of the 830 Ma high-Mg diorites, as well as the high-Mg andesites in the Yiyang area of northern Hunan Province (Zhang et al., 2012b), provides solid evidence for the existence of Neoproterozoic subduction at the western part of the Jiangnan orogen, suggesting that they are part of the subduction system along the southeastern margin of the Yangtze Block. Therefore, the amalgamation between the Yangtze and Cathaysia blocks at the western Jiangnan orogen has not been terminated at ca. 830 Ma, which is consistent with the results of detrital zircons in the Sibao Group and equivalent sedimentary sequences (Li et al., 2011; Wang et al., 2007, 2010, 2012, 2014; Zhou et al., 2009).

7. Conclusions

(1) High-Mg diorites (MgO = 6.7–8.9 wt%) were discovered in the southern part of the ca. 830 Ma Dongma Pluton, northern Guangxi Province of southern China. They show high Mg-number, Cr and Ni concentrations and enriched and varied Nd-Hf isotopes, contrasting to the associated medium- to low-Mg granodiorites.

(2) The high-Mg diorites are geochemically similar to the arc volcanic HMAs (boninites and Setouchi high-Mg andesites) but different from typical adakites. They are generated from the mixing of melts from partial melting of metasomatized refractory harzburgite mantle and crust-derived low-MgO melts.

(3) The occurrence of high-Mg diorites implies the existence of subduction-related metasomatism in the western part of the Jiangnan orogen at ca. 830 Ma.

Acknowledgements

This work was financially supported by the National Natural Science Foundation of China (Grant No. 41222016), a 973 project of China (2012CB416701) and the China Geological Survey (No. 12120113065200). We thank M.L. Hou for electron microprobe analyses, L.H. Chen for major element analyses, L. Qi, T. Yang and W. Pu for trace element analyses and Sr-Nd-Hf isotope analyses. We appreciate the thoughtful and constructive comments and corrections from Prof. Gen Shimoda and an anonymous reviewer. This manuscript also benefited discussions with Profs. Jin-Hai Yu and L.H. Chen.

Appendix A. Supplementary data

Supplementary data to this article can be found online at http://dx.doi.org/10.1016/j.lithos.2014.04.007.

References

Arai, S., 1992. Chemistry of chromian spinel in volcanic rocks as a potential guide to magma chemistry. Mineralogical Magazine 56, 173–184.
Barnes, S.J., Roeder, P.L., 2001. The range of spinel composition in terrestrial mafic and ultramafic rocks. Journal of Petrology 42, 2279–2302.
Beeson, M.H., Jackson, E.D., 1969. Chemical composition of altered chromites from the Stillwater Complex, Montana. American Mineralogist 54, 1084–1100.
Carlson, R.W., Boyet, M., Horan, M., 2007. Chondrite barium, neodymium, and samarium isotopic heterogeneity and early earth differentiation. Science 316, 1175–1178.
Carpentier, M., Chauvel, C., Maury, R., Mattielli, N., 2009. The "zircon effect" as recorded by the chemical and Hf isotopic compositions of the Lesser Antilles forearc sediments. Earth and Planetary Science Letters 287, 86–99.
Chu, Z.Y., Chen, F.K., Yang, Y.H., Guo, J.H., 2009. Precise determination of Sm, Nd concentrations and Nd isotopic compositions at the nanogram level in geological samples by thermal ionization mass spectrometry. Journal of Analytical Atomic Spectrometry 24, 1534–1544.
Condie, K.C., 1981. Archean greenstone belts. Elsevier, New York (434 pp.).
Couch, S., Sparks, R.S.J., Carroll, M.R., 2001. Mineral disequilibrium in lavas explained by convective self-mixing in open magma chambers. Nature 411, 1037–1039.
Crawford, A.J., Falloon, T.J., Green, D.H., 1989. Classification, petrogenesis and tectonic setting of boninites. In: Crawford, A.J. (Ed.), Boninites and related rocks. Unwin Hyman, London, pp. 1–49.
Defant, M.J., Drummond, M.S., 1990. Derivation of some modern arc magmas by melting of young subducted lithosphere. Nature 347, 662–665.
Gao, S., Rudnick, R.L., Yuan, H.L., Liu, X., Liu, Y.S., Xu, W.L., Ling, W.L., Ayers, J., Wang, X.C., Wang, Q.H., 2004. Recycling lower continental crust in the North China craton. Nature 432, 892–897.
Ge, W.C., Li, X.H., Li, Z.X., Wang, J., Zhou, H.W., Li, J.Y., 2000. Geological and geochemical evidence for the genesis of tremolitized mafic rocks from Baotan in northern Guangxi. Geochimica 29 (3), 253–258 (in Chinese with English abstract).
Ge, W.C., Li, X.H., Li, Z.X., Zhou, H.W., Li, J.Y., 2001a. Geochemical studies on two types of Neoproterozoic peraluminous granitoids in northern Guangxi. Geochimica 30 (1), 24–34 (in Chinese with English abstract).
Ge, W.C., Li, X.H., Liang, X.R., Wang, R.C., Li, Z.X., Zhou, H.W., 2001b. Geochemistry and geological implications of mafic-ultramafic rocks with the age of ~825 Ma in Yuanbaoshan-Baotan area of northern Guangxi. Geochimica 30 (2), 123–130 (in Chinese with English abstract).
Gill, J.B., 1981. Orogenic andesites and plate tectonics. Springer-Verlag, Berlin.
Grove, T.L., Elkins-Tanton, L.T., Parman, S.W., Chatterjee, N., Münterner, O., Gaetani, G.A., 2003. Fractional crystallization and mantle-melting controls on calc-alkaline differentiation trends. Contributions to Mineralogy and Petrology 145, 515–533.
GXRGST (Guangxi Regional Geological Survey Team), 1995.Regional Geological Survey Report (Sanfang area, 1:50000), 1–225 (in Chinese).
GXRGST(Guangxi Regional Geological Survey Team), 1987. Regional Geological Survey Report (Baotan area, 1:50000), 1–294 (in Chinese).
Hamilton, P.J., O'Nions, R.K., Bridgwater, D., Nutman, A., 1983. Sm-Nd studies of Archaean metasediments and metavolcanics from West Greenland and their implications for the Earth's early history. Earth and Planetary Science Letters 62, 263–272.
Hildreth, W., 1981. Gradients in silicic magma chambers: Implications for lithospheric magmatism. Journal of Geophysical Research 86, 10153–10192.
Hunter, A.G., 1998. Intracrustal controls on the coexistence of tholeiitic and calc-alkaline magma series at Aso Volcano, SW Japan. Journal of Petrology 39, 1255–1284.
Jacobsen, S.B., Wasserburg, G.J., 1984. Sm-Nd isotopic evolution of chondrites and achondrites, II. Earth and Planetary Science Letters 67, 137–150.
Kamei, A., Owada, M., Nagao, T., Shiraki, K., 2004. High-Mg diorites derived from sanukitic HMA magmas, Kyushu Island, southwest Japan arc: Evidence from clinopyroxene and whole rock compositions. Lithos 75, 359–371.
Kamenetsky, V.S., Crawford, A.J., Meffre, S., 2001. Factors controlling chemistry of magmatic spinel: An empirical study of associated olivine, Cr-spinel and melt inclusions from primitive rocks. Journal of Petrology 42 (4), 655–671.
Kawabata, H., Shuto, K., 2005. Magma mixing recorded in intermediate rocks associated with high-Mg andesites from the Setouchi volcanic belt, Japan: Implications for Archean TTG formation. Journal of Volcanology and Geothermal Research 140, 241–271.
Kay, R.W., 1978. Aleutian magnesian andesites: Melts from subducted Pacific Ocean crust. Journal of Volcanology and Geothermal Research 4, 117–132.
Koto, B., 1916. On the volcanoes of Japan (V). Journal of the Geological Society of Tokyo 23, 95–127.
Kuroda, N., Shiraki, K., Urano, H., 1978. Boninite as a possible calc-alkalic primary magma. Bulletin of Volcanology 41, 563–575.
Li, J.P., Provost, A., Kornprobst, J., 1997a. Mechanism of chemical zonation of spinel in peridotite and its geological significance. Acta Mineralogica Sinica 17, 156–163 (in Chinese with English abstract).
Li, X.H., Zhao, J.X., McCulloch, M.T., Zhou, G.Q., Xing, F.M., 1997b. Geochemical and Sm-Nd isotopic of Neoproterozoic ophiolites from southeastern China: Petrogenesis and tectonic implications. Precambrian Research 81, 129–144.

Li, X.H., Li, Z.X., Ge, W.C., Zhou, H.W., Li, W.X., Liu, Y., Wingate, M.T.D., 2003a. Neoproterozoic granitoids in South China: Crustal melting above a mantle plume at ca. 825 Ma? Precambrian Research 122, 45–83.
Li, Z.X., Li, X.H., Kinny, P.D., Wang, J., Zhang, S., Zhou, H., 2003b. Geochronology of Neoproterozoic syn-rift magmatism in the Yangtze Craton, South China and correlations with other continents: Evidence for a mantle superplume that broke up Rodinia. Precambrian Research 122, 85–109.
Li, X.H., Li, Z.X., Ge, W.C., Zhou, H.W., Li, W.X., Liu, Y., Wingate, M.T.D., 2004. Reply to the comment: Mantle plume-, but not arc-related neoproterozoic magmatism in South China. Precambrian Research 132, 405–407.
Li, X.H., Li, W.X., Li, Z.X., Lo, C.H., Wang, J., Ye, M.F., Yang, Y.H., 2009. Amalgamation between the Yangtze and Cathaysia Blocks in South China: Constraints from SHRIMP U-Pb zircon ages, geochemistry and Nd-Hf isotopes of the Shuangxiwu volcanic rocks. Precambrian Research 174, 117–128.
Li, L.M., Sun, M., Wang, Y.J., Xing, G.F., Zhao, G.C., He, Y.H., He, K.J., Zhang, A.M., 2011. U-Pb and Hf isotopic study of detrital zircons from the meta-sedimentary rocks in central Jiangxi Province, South China: Implications for the Neoproterozoic tectonic evolution of South China Block. Journal of Asian Earth Sciences 41, 44–55.
Macpherson, C.G., Hall, R., 2001. Tectonic setting of Eocene boninite magmatism in the Izu- Bonin- Mariana forearc. Earth and Planetary Science Letters 186, 215–230.
McDonough, W.F., Sun, S.-S., 1995. The composition of the earth. Chemical Geology 120, 223–253.
Moyen, J.F., Martin, H., Jayananda, M., Auvray, B., 2003. Late Archaean granites: A typology based on the Dharwar Craton (India). Precambrian Research 127, 103–123.
Nyquist, L.E., Bansal, B., Wiesmann, H., Shih, C.-Y., 1994. Neodymium, strontium and chromium isotopic studies of the LEW86010 and Angra dos Reis meteorites and the chronology of the angrite parent body. Meteoritics 29, 872–885.
Qian, Q., Hermann, J., 2010. Formation of high-Mg diorites through assimilation of peridotite by monzodiorite magma at crustal depths. Journal of Petrology 51 (7), 1381–1416.
Qiu, J.S., Zhou, J.C., Zhang, G.H., Ling, W.L., 2002. Geochemistry and petrogenesis of Precambrian granitoid rocks in northern Guangxi. Acta Petrologica et Mineralogica 21 (3), 197–208 (in Chinese with English abstract).
Rapp, R.P., Shimizu, N., Norman, M.D., 2003. Growth of early continental crust by partial melting of eclogite. Nature 425, 605–609.
Rapp, R.P., Norman, M.D., Laporte, D., Yaxley, G.M., Martin, H., Foley, S.F., 2010. Continental formation in the Archean and chemical evolution of the cratonic lithosphere: Melt-rock reaction experiments at 3-4GPa and petrogenesis of Archean Mg-diorites. Journal of Petrology 52 (6), 1237–1266.
Rogers, N.W., Hawkesworth, C.J., Parker, R.J., Marsh, J.S., 1985. The geochemistry of potassic lavas from Vulsini, central Italy and implications for mantle enrichment processes beneath the Roman region. Contributions to Mineralogy and Petrology 90, 244–257.
Rudnick, R.L., Fountain, D.M., 1995. Nature and composition of the continental crust: A lower crustal perspective. Reviews of Geophysics 33, 267–309.
Rudnick, R.L., Gao, S., 2004. Composition of the continental crust. In: Rudnick, R.L., Holland, H.D., Turekian, K.K. (Eds.), The crust. Treatise on Geochemistry, vol. 3. Elsevier-Pergaman, Oxford, pp. 1–64.
Sakuyama, M., 1981. Petrological study of the Myoko and Kurohime volcanoes, Japan: Crystallization sequence and evidence for magma mixing. Journal of Petrology 22, 553–583.
Saunders, A.D., Rogers, G., Marriner, G.F., Terrell, D.J., Verma, S.P., 1987. Geochemistry of Cenozoic volcanic rocks, Baja California, Mexico: Implications for the petrogenesis of postsubduction magmas. In: Weaver, S.D., Johnson, R.W. (Eds.), Tectonic Controls on Magma Chemistry. Elsevier, Amsterdam, pp. 223–245.
Shimoda, G., 2009. Genetic link between EMI and EMII: An adakite connection. Lithos 112, 591–602.
Shimoda, G., Tatsumi, Y., 1999. Generation of rhyolite magmas by melting of subducting sediments in Shodo-shima Island, SW Japan, and its bearing on the origin of high-Mg andesites. Island Arc 8, 383–392.
Shimoda, G., Tatsumi, Y., Nohda, S., Ishizaka, K., Jahn, B.M., 1998. Setouchi high-Mg andesites revisited: Geochemical evidence for melting of subducting sediments. Earth and Planetary Science Letters 160, 479–492.
Shimoda, G., Tatsumi, Y., Morishita, Y., 2003. Behavior of subducting sediments beneath an arc under high geothermal gradient: Constraints from the Miocene SW Japan arc. Geochemical Journal 37, 503–518.
Shirey, S.B., Hanson, G.N., 1984. Mantle-derived Archaean monzodiorites and trachyandesites. Nature 310, 222–224.
Stein, M., Starinsky, A., Katz, A., Goldstein, S.L., Machlus, M., Schramm, A., 1997. Strontium isotopic, chemical, and sedimentological evidence for the evolution of Lake Lisan and the Dead Sea. Geochimica et Cosmochimica Acta 61, 3975–3992.
Stern, C.R., Kilian, R., 1996. Role of the subduction slab, mantle wedge and continental crust in the generation of adakites from the Andean Austral Volcanic Zone. Contributions to Mineralogy and Petrology 123, 263–281.
Stern, R.A., Hanson, G.N., Shirey, S.B., 1989. Petrogenesis of mantle-derived, LILE-enriched Archean monzodiorites and trachyandesites (sanukitoids) in southwestern Superior Province. Canadian Journal of Earth Sciences 26, 1688–1712.
Sun, Y.X., 1982. Petrogenesis of granitoids in the Bendong Pluton. Master's thesis Nanjing University (in Chinese).
Sun, S.S., McDonough, W.F., 1989. Chemical and isotopic systematics of oceanic basalt: Implications for mantle composition and processes. In: Saunders, A.D., Norry, M.J. (Eds.), Magmatism in the ocean basins: Geological Society of London Special Publication 42, 313–345.
Tang, M., Wang, X.-L., Shu, X.-J., Wang, D., Yang, T., 2014. Hafnium isotopic heterogeneity in zircons from granitic rocks: Geochemical evaluation and modeling on "zircon effect" in crustal anatexis. Earth and Planetary Science Letters 389, 188–199.
Tatsumi, Y., 1982. Origin of high-magnesian andesites in the Setouchi volcanic belt, southwest Japan II: Melting experiments at high pressures. Earth and Planetary Science Letters 60, 305–317.
Tatsumi, Y., 2006. High-Mg andesites in the Setouchi volcanic belt, southwestern Japan: Analogy to Archean magmatism and continental crust formation? Annual Review of Earth and Planetary Sciences 34, 467–499.
Tatsumi, Y., Ishizaka, K., 1981. Existence of andesitic primary magma: An example from Southwest Japan. Earth and Planetary Science Letters 53, 124–130.
Tatsumi, Y., Maruyama, S., 1989. Boninites and high-Mg andesites: Tectonics and petrogenesis. In: Crawford, A.J. (Ed.), Boninites and related rocks. Unwin Hyman, London, pp. 50–71.
Tatsumi, Y., Nakashima, T., Tamura, Y., 2002. The petrology and geochemistry of calc-alkaline andesites on Shodo-Shima Island, SW Japan. Journal of Petrology 43, 3–16.
Tatsumi, Y., Suzuki, T., Kawabata, H., Sato, K., Miyazaki, T., Chang, Q., Takahashi, T., Tani, K., Shibata, T., Yoshikawa, M., 2006. The petrology and geochemistry of Oto-Zan composite lava flow on Shodo-Shima Island, SW Japan: Remelting of a solidified high-Mg andesite magma. Journal of Petrology 47 (3), 595–629.
Taylor, S.R., McLennan, S.M., 1981. The composition and evolution of the continental crust: Rare earth element evidence from sedimentary rocks. Philosophical Transactions of the Royal Society A 301, 381–399.
Taylor, R.N., Nesbitt, R.W., Vidal, P., Harmon, R.S., Auvray, B., Croudace, I.W., 1994. Mineralogy, chemistry and genesis of the boninite series volcanics, Chichijima, Bonin Islands, Japan. Journal of Petrology 35, 577–617.
Temel, A., Gündogdu, M.N., Gourgaud, A., 1998. Petrological and geochemical characteristics of Cenozoic high-K calc-alkaline volcanism in Konya, Central Anatolia, Turkey. Journal of Volcanology and Geothermal Research 85, 327–354.
Tsuchiya, N., Suzuki, S., Kimura, J.-I., Kagami, H., 2005. Evidence for slab melt/mantle reaction: Petrogenesis of early Cretaceous and Eocene high-Mg andesites from the Kitakami Mountains, Japan. Lithos 79, 179–206 (–129).
Vervoort, J.D., Patchett, P.J., Albarède, F., Toft, J.B., Rudnick, R., Downes, Hilary., 2000. Hf-Nd isotopic evolution of the lower crust. Earth and Planetary Science Letters 181, 115–129.
Wang, D.Z., Zhou, X.M., Sun, Y.X., 1982. Basic characteristics of Precambrian mantle-derived granitoids in South China. Journal of Guilin Institute of Techonology 4, 1–8 (in Chinese).
Wang, X.L., Zhou, J.C., Qiu, J.S., Gao, J.F., 2004a. Comment on "Neoproterozoic granitoids in South China: Crustal melting above a mantle plume at ca. 825 Ma?" by Xian-Hua Li et al. (PR 122, 45–83, 2003). Precambrian Research 132, 405–407.
Wang, X.L., Zhou, J.C., Qiu, J.S., Gao, J.F., 2004b. Geochemistry of the Meso- to Neoproterozoic basic-acid rocks from Hunan Province, South China: Implications for the evolution of the western Jiangnan orogen. Precambrian Research 135, 79–103.
Wang, X.L., Zhou, J.C., Qiu, J.S., Zhang, W.L., Liu, X.M., Zhang, G.L., 2006. LA-ICP-MS U-Pb zircon geochronology of the Neoproterozoic igneous rocks from Northern Guangxi, South China: Implications for petrogenesis and tectonic evolution. Precambrian Research 145 (1–2), 111–130.
Wang, X.L., Zhou, J.C., Griffin, W.L., Wang, R.C., Qiu, J.S., O'Reilly, S.Y., Xu, X.S., Liu, X.M., Zhang, G.L., 2007. Detrital zircon geochronology of Precambrian basement sequences in the Jiangnan orogen: Dating the assembly of the Yangtze and Cathaysia blocks. Precambrian Research 159 (1–2), 117–131.
Wang, X.L., Zhou, J.C., Qiu, J.S., Jiang, S.Y., Shi, Y.R., 2008. Geochronology and geochemistry of Neoproterozoic mafic rocks from western Hunan, South China: Implications for petrogenesis and post-orogenic extension. Geological Magazine 145 (2), 215–233.
Wang, L.J., Griffin, W.L., Yu, J.H., O'Reilly, S.Y., 2010. Precambrian crustal evolution of the Yangtze Block tracked by detrital zircons from Neoproterozoic sedimentary rocks. Precambrian Research 177, 131–144.
Wang, W., Zhou, M.F., Yan, D.P., Li, J.W., 2012. Depositional age, provenance, and tectonic setting of the Neoproterozoic Sibao Group, southeastern Yangtze Block, South China. Precambrian Research 192–195, 107–124.
Wang, D., Wang, X.L., Zhou, J.C., Shu, X.J., 2013a. Unravelling the Precambrian crustal evolution by Neoproterozoic basal conglomerates, Jiangnan orogen: U-Pb and Hf isotopes of detrital zircons. Precambrian Research 233, 223–236.
Wang, X.L., Zhou, J.C., Wan, Y.S., Kitajima, K., Wang, D., Bonamici, C., Qiu, J.S., Sun, T., 2013b. Magmatic evolution and crustal recycling for Neoproterozoic strongly peraluminous granitoids from southern China: Hf and O isotopes in zircon. Earth and Planetary Science Letters 366, 71–82.
Wang, X.L., Zhou, J.C., Griffin, W.L., Zhao, G.C., Yu, J.H., Qiu, J.S., Zhang, Y.J., Xing, G.F., 2014. Understanding the contrasting geochemical features of the crust in the Jiangnan Orogen. Precambrian Research 242, 154–171.
White, R.W., 1966. Ultramafic inclusions in basaltic rocks from Hawaii. Contributions to Mineralogy and Petrology 12, 245–314.
Wood, B.J., Turner, S., 2009. Origin of primitive high-Mg andesite: Constraints from natural examples and experiments. Earth and Planetary Science Letters 283, 59–66.
Wu, R.X., Zheng, Y.F., Wu, Y.B., Zhao, Z.F., Zhang, S.B., Liu, X.M., Wu, F.Y., 2006. Reworking of juvenile crust: Element and isotope evidence from Neoproterozoic granodiorite in South China. Precambrian Research 146, 179–212.
Xu, W.L., Yang, D.B., Gao, S., Pei, F.P., Yu, Y., 2010. Geochemistry of peridotite xenoliths in Early Cretaceous high-Mg# diorites from the Central Orogenic Block of the North China Craton: The nature of Mesozoic lithospheric mantle and constraints on lithospheric thinning. Chemical Geology 270, 257–273.
Yang, Y.H., Zhang, H.F., Chu, Z.Y., Xie, L.W., Wu, F.Y., 2010. Combined chemical separation of Lu, Hf, Rb, Sr, Sm and Nd from a single rock digest and precise and accurate isotope determinations of Lu-Hf, Rb-Sr and Sm-Nd isotope systems using Multi-Collector ICP-MS and TIMS. International Journal of Mass Spectrometry 290, 120–126.
Yin, J.Y., Yuan, C., Sun, M., Long, X.P., Zhao, G.C., Wong, K.P., Geng, H.Y., Cai, K.D., 2010. Late carboniferous high-Mg dioritic dikes in Western Junggar, NW China: Geochemical features, petrogenesis and tectonic implications. Gondwana Research 17, 145–152.

Yogodzinski, G.M., Volynets, O.N., Koloskov, A.V., Seliverstov, N.I., Matvenkov, V.V., 1994. Magnesian andesites and the subduction component in a strongly calc-alkaline series at Piip Volcano, far western Aleutians. Journal of Petrology 35, 163–204.
Yogodzinski, G.M., Kay, R.W., Volynets, O.N., Koloskov, A.V., Kay, S.M., 1995. Magnesian andesite in the western Aleutian Komandorsky region: Implications for slab melting and processes in the mantle wedge. Geological Society of America Bulletin 107, 505–519.
Zhang, S.B., Wu, R.X., Zheng, Y.F., 2012a. Neoproterozoic continental accretion in South China: Geochemical evidence from the Fuchuan ophiolite in the Jiangnan orogen. Precambrian Research 220–221, 45–64.
Zhang, Y.Z., Wang, Y.J., Fan, W.M., Zhang, A.M., Ma, L.Y., 2012b. Geochronological and geochemical constraints on the metasomatised source for the Neoproterozoic (~825 Ma) high-mg volcanic rocks from the Cangshuipu area (Hunan Province) along the Jiangnan domain and their tectonic implications. Precambrian Research 220–221, 139–157.
Zhao, G.C., Cawood, P.A., 2012. Precambrian geology of China. Precambrian Research 222–223, 13–54.
Zhao, Z.J., Ma, D.Q., Lin, H.K., Yuan, C.L., Zhang, X.H., 1987. A study on the Precambrian granitoids from Bendong and Sanfang massifs, Northern Guangxi. Yichang Institute of Geology, Mineral, Resources, Research Reports of the Geology, Mineral, pp. 1–27 (in Chinese with English abstract).
Zhao, J.H., Zhou, M.F., Zheng, J.P., Fang, S.M., 2010. Neoproterozoic crustal growth and reworking of the Northwestern Yangtze Block: Constraints from the Xixiang dioritic intrusion, South China. Lithos 120, 439–452.
Zheng, Y.-F., Zhang, S.-B., Zhao, Z.-F., Wu, Y.-B., Li, X., Li, Z., Wu, F.-Y., 2007. Contrasting zircon Hf and O isotopes in the two episodes of Neoproterozoic granitoids in South China: Implications for growth and reworking of continental crust. Lithos 96, 127–150.
Zheng, Y.-F., Wu, R.X., Wu, Y.-B., Zhang, S.-B., Yuan, H.L., Wu, F.-Y., 2008. Rift melting of juvenile arc-derived crust: Geochemical evidence from Neoproterozoic volcanic and granitic rocks in the Jiangnan Orogen, South China. Precambrian Research 163, 351–383.
Zhou, M.F., Zhao, T.P., Malpas, J., Sun, M., 2000. Crustal contaminated komatiitic basalts in southern China: Products of a Proterozoic mantle plume beneath the Yangtze block. Precambrian Research 103, 175–189.
Zhou, J.C., Wang, X.L., Qiu, J.S., Gao, J.F., 2004. Geochemistry of Meso- and Neoproterozoic mafic- ultramafic rocks from northern Guangxi, China: Arc or plume magmatism? Geochemical Journal 38, 139–152.
Zhou, J.B., Li, X.H., Ge, W.C., Li, Z.X., 2007. Age and origin of middle Neoproterozoic mafic magmatism in southern Yangtze Block and relevance to the break-up of Rodinia. Gondwana Research 12, 184–197.
Zhou, J.C., Wang, X.L., Qiu, J.S., 2009. Geochronology of Neoproterozoic mafic rocks and sandstones from northeastern Guizhou, South China: Coeval arc magmatism and sedimentation. Precambrian Research 170, 27–42.